Journal of Nanoparticle Research (2006) 8: 681–692
DOI 10.1007/s11051-006-9136-z

Reflectance spectroscopy of gold nanoshells: computational predictions and experimental measurements

Alex W. H. Lin, Nastassja A. Lewinski, Min-Ho Lee and Rebekah A. Drezek*
*Department of Bioengineering, Rice University, MS-142, P.O. Box 1892, Houston, TX, 77251-1892, USA; *Author for correspondence (Tel.: +1-713-348-3011; Fax: +1-713-348-5877; E-mail: drezek@rice.edu)*

Received 27 February 2006; accepted in revised form 14 June 2006

Key words: nanoshells, nanoparticles, Monte Carlo, contrast agents, reflectance, spectroscopy, modeling and simulation

Abstract

Gold nanoshells are concentric spherical constructs that possess highly desirable optical responses in the near infrared. Gold nanoshells consist of a thin outer gold shell and a silica core and can be used for both diagnostic and therapeutic purposes by tuning the optical response through changing the core–shell ratio as well as the overall size. Although optical properties of gold nanoshells have already been well documented, the reflectance characteristics are not well understood and have not yet been elucidated by experimental measurements. Yet, in order to use gold nanoshells as an optical contrast agent for scattering-based optical methods such as reflectance spectroscopy, it is critical to characterize the reflectance behavior. With this in mind, we used a fiber-optic-based spectrometer to measure diffuse reflectance of gold nanoshell suspensions from 500 nm to 900 nm. Experimental results show that gold nanoshells cause a significant increase in the measured reflectance. Spectral features associated with scattering from large angles (~180°) were observed at low nanoshell concentrations. Monte Carlo modeling of gold nanoshells reflectance demonstrated the efficacy of using such methods to predict diffuse reflectance. Our studies suggest that gold nanoshells are an excellent candidate as optical contrast agents and that Monte Carlo methods are a useful tool for optimizing nanoshells best suited for scattering-based optical methods.

Abbreviations: NIR: near infrared; OCT: optical coherence tomography; CCD: charge-coupled device; POI: point of photon insertion; LAS: large angle scattering

Introduction

Presently, diagnostic procedures to detect the presence of cancerous tissue often include painful biopsies, time-consuming histopathological analysis, and conventional imaging techniques that use potentially harmful ionizing radiation. However, utilizing advanced optical technologies, such as those proposed within the scope of this paper, within the spectrum of cancer diagnostics can prove beneficial in several important ways. First, small and subtle changes in optical properties associated with early cancers are difficult to discern from normal tissue (Drezek et al., 2003), using either the current conventional or optical technologies. Second, advances in optical technologies for cancer diagnostics also promise to improve sensitivity, specificity, and cost effectiveness, as well as bring higher resolution and non-invasive imaging and assessment of tissue over current approaches.

Specifically, scattering-based optical techniques, such as polarized scattering spectroscopy (Sokolov et al., 2004) and optical coherence tomography

(OCT) (Matheny et al., 2004), utilize intrinsic changes, including increased nuclear size and changes in refractive index, to differentiate normal from diseased tissue. These methods have shown considerable promise in overcoming limitations associated with current optical techniques. However, these changes, and many other valuable molecular indicators of early cancers, may not, at the same time, generate obvious intrinsic optical contrast. For this reason, optical contrast agents that can, in fact, enhance the subtle differences between normal and diseased tissue by targeting specific biomolecular markers of interest are most desirable for the early detection of cancer.

Various chemical and particle-based techniques have been investigated for use as contrast agents for optical technologies (Brigger et al. 2002; Licha, 2002; West & Halas, 2003). However, as optical diagnosis of cancer is still a developing field, the use of such agents is not routine. Particle-based technologies have generated much interest for enhancing contrast for optical imaging (Sokolov et al., 2003; Loo et al., 2004a, b) and microscopy (Loo et al., 2004a, b; Wang et al., 2004) due to their unique optical capabilities and ease of adding surface modifications. However, with the advancement in nanotechnology, interest is rapidly growing in developing nanoparticle-based contrast agents to probe for and target molecular signatures of interest. This exciting nexus of nano-bio-opto technologies aims to improve detecting, monitoring and sensing of biomolecules that can potentially achieve earlier and greater accuracy in cancer detection. Molecular-specific contrast agents achieve specific targeting through antibody binding of tumor cell surface molecules or tumor-specific peptides. Antibody targeting has been used extensively to achieve cell-selective targeting by therapeutic and diagnostic agents, and it is especially useful for targeting biomarkers of cancers (Chen et al., 2005; Michalet et al., 2005). To illustrate, Chen et al. (2005) showed OCT image enhancement using gold nanocages and have also targeted breast cancer cells through the process of bioconjugation. Levy et al. (2002) used targeted silica, encapsulating magnetic nanoparticles and fluorescent dyes, to enhance optical imaging and, therefore, the detection and therapy of oral cancer cells. In addition, nanoparticles, such as semiconductor quantum dots, also have highly modifiable surfaces and show similar potential for use as target-specific probes (Akerman et al., 2002; Wang et al., 2004). Chang et al. (2005), for example, showed the utility of using protease-activated quantum dots to potentially improve bioimaging of protease activity.

In this paper, though, we consider the use of metal nanoshells as an exogenous contrast agent. Metal nanoshells consist of a dielectric core, typically silica, covered with a thin outer metallic shell, usually gold. Gold nanoshells exhibit enhanced scattering and absorption behavior due to the strong plasmon resonance of the metallic-dielectric concentric spherical configuration (Oldenburg et al., 1998). In particular, the optical behavior of gold nanoshells in the near infrared (NIR) wavelengths shows scattering and/or absorption cross sections several times the particle geometric cross section (Oldenburg et al., 1999). This is not seen with comparable particles such as gold colloidal nanoparticles, which show weak optical activity in the NIR spectrum region (Kreibig & Vollmer, 1995). By varying the relative core size and shell thickness, the peak resonance of the gold nanoshells can be systematically varied across a broad range of the optical spectrum that spans the visible and the near infrared spectral regions. In Figure 1, Mie extinction plots are shown with a 50 nm radius silica core and an increasing core radius-to-shell thickness ratio that shifts the peak resonance into the NIR. Gold nanoshells can also be tuned to preferentially absorb or scatter at the same peak optical resonance (Loo et al., 2004a, b). Under current laboratory methods, it is possible to fabricate gold nanoshells of varying sizes with experimental observations of optical attenuation closely matching Mie theory. The fabrication method utilizes a combination of molecular self-assembly and colloid chemistry in aqueous solution.

The strong optical responses of gold nanoshells in the NIR are especially useful for biophotonic applications where medium optical transmissivity peaks. Gold nanoshell surfaces are virtually chemically identical to gold colloid used in numerous bioconjugate applications (Faulk & Taylor, 1971). By functionalizing gold nanoshell surfaces with target-specific antibodies, Loo et al. (2004a, b) showed that visualization of HER2-positive breast cancer cells under brightfield and darkfield microscopy could be enhanced using HER2-targeting gold nanoshells. The targeted cancer cells can then be selectively destroyed via

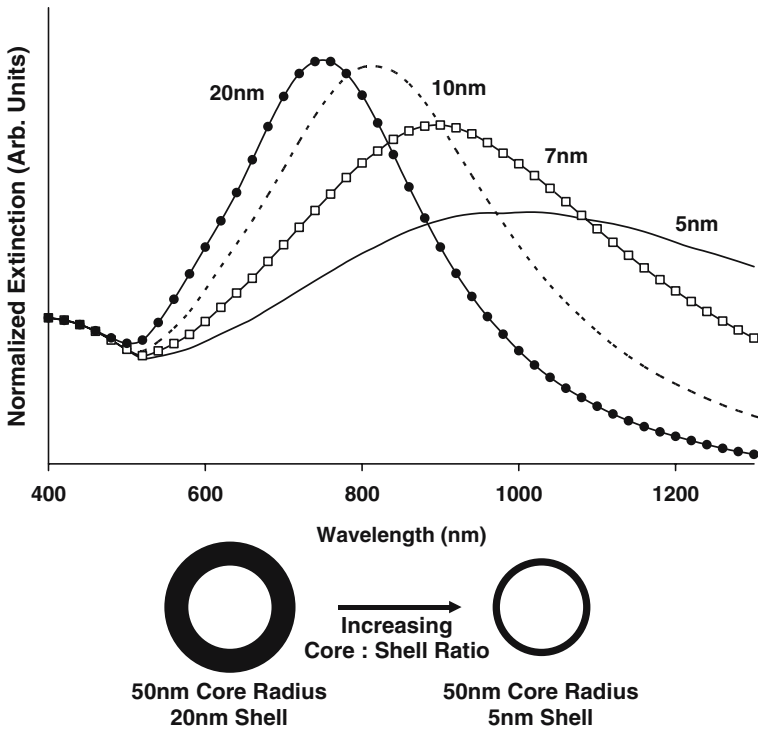

Figure 1. By increasing the core radius-to-shell thickness ratio, the peak extinction resonance can be shifted well into the NIR. Peak resonance shifts to longer wavelengths for gold nanoshells with a core (silica) radius of 50 nm and a decreasing gold shell thickness.

photothermal destruction (Loo et al., 2005). Although gold nanoshells have already shown considerable success in both cancer imaging and therapy, the reported optical properties of nanoshells thus far show only properties in transmission, and experimental measurements have not yet been reported for reflectance. Characterizing nanoshell reflectance is, therefore, a crucial step in understanding how gold nanoshells affect tissue reflectance for scattering-based optical methods. This will, in turn, help in further elucidating the efficacy of gold nanoshells as an optical contrast agent.

Using experimental and computational tools, we evaluated diffuse reflectance behavior of gold nanoshells suspended in water. We first used analytical electromagnetic methods to calculate optical properties of various nanoshells with a variety of scattering and absorbing capabilities. Subsequently, we measured diffuse reflectance of gold nanoshell suspensions of varying concentrations using a fixed geometry fiber-probe-based spectrometer. To investigate the efficacy of using computational methods to predict reflectance from nanoparticle suspensions, Monte Carlo methods were used to model diffuse reflectance from computer models based on these same gold nanoshell suspensions. It should be further noted that Monte Carlo methods have been widely used to simulate photon propagation through a turbid medium, such as biological tissue (Wang et al., 1995). As such, the use of these methods can also assist in evaluating predictions of macroscopic reflectance behavior of nanoparticles, such as gold nanoshells, in a turbid medium.

Based on our studies, we show that the measured diffuse reflectance from gold nanoshell suspensions can be efficiently modeled with Monte Carlo methods. In general, reflectance is greater with high scattering, low absorption and low anisotropy of nanoshells (greater probability of scattering backwards). Due to the fixed fiber-probe geometry, spectral features related to scattering from large angles ($\sim$180°) become more noticeable at lower nanoshell concentrations. As a result, scattering from large angles results in higher

measured reflectance and may be a useful feature for detecting the presence of nanoshells at low concentrations. However, at the same time, the accuracy of computational predictions may be limited. The Monte Carlo models cannot account for the rise in detection of photons that are singly scattered at large angles (~180°), as the assumption that gold nanoshells gives rise to a homogenous change in optical properties of the medium, may not be accurate at low concentrations of nanoshells.

Methods

Gold nanoshells have been shown by various investigators to possess unique properties for use as an optical contrast agent and also as a therapeutic agent for cancer diagnosis and treatment (Loo et al., 2005). To non-invasively detect early cancers, using gold nanoshells as a scattering-based optical contrast agent, there is a need to understand how gold nanoshells affect diffuse reflectance.

Optical properties of gold nanoshells

The optical response of gold nanoshells can be described by using computed solutions of Mie theory for concentric spherical shells at the boundaries between different mediums: the gold shell, the silica core, and the embedding medium (Oldenburg et al., 1999). To investigate how optical properties of gold nanoshells affect diffuse reflectance, theoretical optical properties of gold nanoshells were first calculated with excitation wavelengths from 500 nm to 900 nm in water ($n = 1.33$). Using Mie scattering solutions at 180° (opposite direction to the excitation wave direction), the scattering efficiencies were calculated to examine the effect of scattering from large angles on reflectance. To avoid confusion, in this paper, theoretical scattering efficiency from 180° will subsequently be called the Q_{180} scattering efficiency. From Mie Theory, the Q_{180} efficiency is given as

$$Q_{180} = \frac{4}{k^2 r^2} |S_{11}(180^\circ)| \quad \text{where } k = \frac{2\pi n}{\lambda}, r = \text{radius} \tag{1}$$

The term $S_{11}(180^\circ)$ is the Mie angular scattering component in the direction opposite of the excitation plane wave (van der Hulst, 1981; Bohren and Huffman, 1983). Gold nanoshells of approximately R71/84 (representing a core radius of 71 nm and total radius of 84 nm), R104/127 and R154/178, all showing different optical properties, were selected and used for the Monte Carlo studies and fabricated for spectroscopic measurements.

Gold nanoshell fabrication

Gold nanoshells of a wide range of sizes can, with adequate predictability and reproducibility, be fabricated using current laboratory protocols. First, the silica cores were made by reducing tetraethylorthosilicate (Sigma-Aldrich) in ethanol as outlined by Stober et al. (1968). The average size of the silica core nanoparticles were then determined by scanning electron microscopy, SEM (Philips FEI XL30). The surface of the Stober particles were then functionalized with amine groups using 3-aminopropylethoxysilane (Sigma-Aldrich). To form the outer gold shell, the aminated silica particles were added to concentrated, aged (2 weeks at ~4 °C) gold colloid that was grown using the method outlined by Duff & Baker (1993). The gold colloid adsorbs onto the aminated surface and forms nucleation sites for the further reduction of gold onto the Stober nanoparticle surface. The gold shell was then grown by reacting $HAuCl_4$ (Sigma-Aldrich) with the gold-seeded aminated particles in the presence of formaldehyde. The absorbance characteristics of the nanoshells were monitored using a UV–Vis spectrophotometer. The average size and distribution of the gold nanoshells were then measured using the SEM and the standard deviations of the nanoshell sizes were determined to be approximately 5%. The sizes of the nanoshells were then reconfirmed by comparing the UV–VIS measurements and the theoretical Mie extinction at the average size. Gold nanoshells of average sizes approximately R71/84 (representing a core radius of 71 nm and an overall radius of 84 nm), R104/127 and R154/178 were fabricated to encompass a variety of different optical properties. Figure 2 shows a SEM micrograph of the R154/178 gold nanoshell, one of the nanoshells fabricated for the spectroscopy studies. The gold nanoshell suspensions were concentrated to a

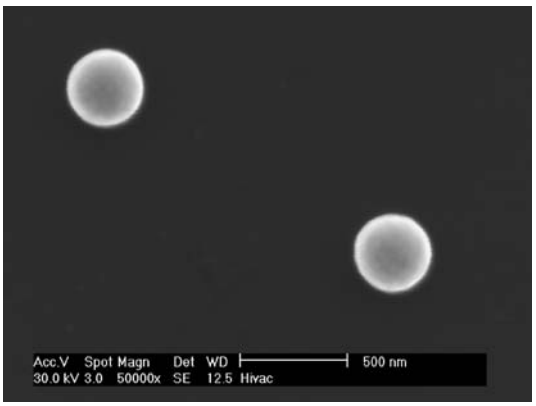

Figure 2. Scanning electron microscope (SEM) image of the R154/178 (representing a core radius of 154 nm and overall radius of 178 nm) nanoshell. The scale bar represents 500 μm.

volume fraction of approximately 0.0002 for spectroscopic measurements.

Diffuse reflectance spectroscopy

Diffuse reflectance measurements of nanoshell suspensions were performed using a fiber-optic-based Ocean Optics HR2000 spectrometer (Ocean Optics, Inc., Dunedin, FL). The instrument consists of a tungsten-halogen broadband light source (DH2000, Ocean Optics, Inc.) and a spectrometer (HR2000, Ocean Optics, Inc.) with a 2048 element charge-coupled device (CCD) (UV2/OFLV-5, Ocean Optics, Inc.). The spectrometer has a slit width of 5 μm with the optical resolution of approximately 0.66 nm. The instrument was set up to collect diffuse reflectance of nanoshell suspensions from 500 nm to 900 nm through a fiber optic reflection probe. The illumination and collection is coupled through a fiber probe consisting of six illumination fibers around one read fiber (R400-ANGLE, Ocean Optics, Inc.). Each fiber is 400 μm in diameter with a numerical aperture of 0.22, and the probe end employs a 30° glass window to eliminate specular reflectance. The charge-coupled device in the spectrometer detects reflected light and presents the intensity as a function of wavelength. A diffuse reflection standard (WS-1, Ocean Optics, Inc.) submerged in water was used as the 100% reflectance reference. The angled probe was placed approximately 0.3 cm above the surface of the reference and the detected reflectance was referenced as 100% reflectance with an integration time of 700 ms. This process ensures maximum detection of reflected photons without detector saturation. A darkened cuvette with water was used as the base reference (0% reflectance) with the probe immersed and illumination turned on. Suspensions of gold nanoshells were measured with a starting volume fraction (V_f) of ~0.0002 and subsequently diluted by 5×, 25×, and 100×. Each suspension was measured using a darkened cuvette with the probe immersed in the nanoshell suspension and the percent diffuse reflectance recorded with an integration time of 700 ms.

Monte Carlo modeling

Photon propagation through a turbid medium, such as biological tissue, can be efficiently modeled using Monte Carlo methods. The method allows investigators to accurately predict how light interacts with tissue without the use of actual biological tissue. Monte Carlo modeling of photon transport by Wang et al. (1995), a computational tool written in Standard C (MCML), has been widely used to simulate the random walk of photons through multilayered turbid media. Scattering and absorption events of photons propagating through a turbid medium can be accurately modeled using this method. Then, as optical parameters, such as scattering and absorption coefficients of the model, are changed, the propagation behavior changes accordingly. In our study, diffuse reflectance from a suspension of nanoshells in water was modeled as a homogenous medium. Following the method shown by Lin et al. (2005), the scattering and absorption cross sections (C) of gold nanoshells can be related to the scattering (μ_{sca}) and absorption coefficients (μ_{abs}) by

$$\mu_{sca,abs} = N \times C \quad (2)$$

where N is the number of particles per unit volume. The scattering and absorption coefficients can then be used in the Monte Carlo simulations. To simulate the diffuse reflectance from gold nanoshell suspensions, the embedding medium index of refraction was set at $n = 1.33$ (water) and $n = 1.5$ (glass) for the source medium. To efficiently model and study the diffuse reflectance measured from the experimental measurements, we employed the use of a simplified Monte Carlo model to simulate diffuse reflectance from a gold

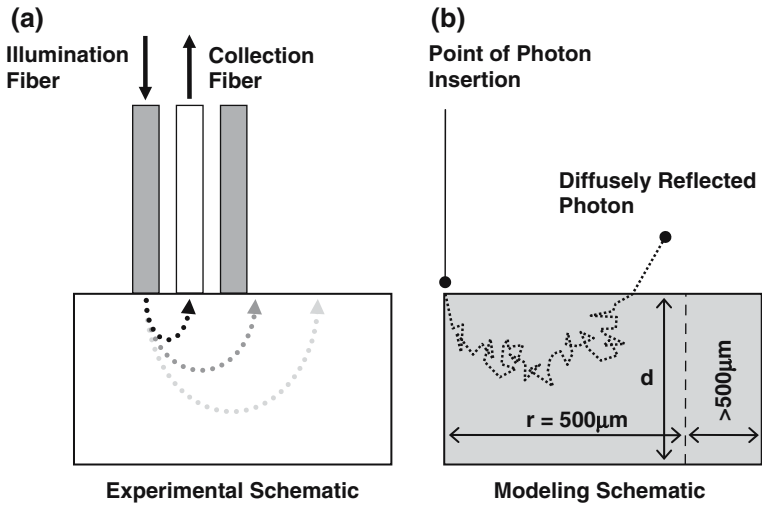

Figure 3. Schematic shows the (a) experimental setup and (b) the simplified model used in the Monte Carlo studies. Schematic (a) shows the use of the 6-illumination around 1-collection fiber optic probe. Gold nanoshell suspensions were modeled as a homogenous bulk semi-infinite layer ($d = 1.0 \times 10^8$ cm) at the point where photons are introduced (POI) into the model at 0 μm shown in (b). The distribution of photon reflectance was analyzed up to $r = 500$ μm, and all the photons that were remitted at radii > 500 μm were tallied. The total diffuse reflectance, regardless of the distribution, was used in comparison to the experimental results.

nanoshell suspension. Figure 3 shows the experimental (Figure 3(a)) and modeling (Figure 3(b)) schematic, where the collection geometry of the fiber optic probe used in the experimental measurements was simplified and the modeled diffuse reflectance is collected regardless of where the photon is remitted. The modeled diffuse reflectance will be compared to the experimental measurements, followed by an analysis of the radial distribution of the modeled photon reflectance. The scattering and absorption coefficients of the gold nanoshells at the average size of R71/84, R104/127 and R154/178 were calculated with volume fractions of 0.0002 (1×), 4×10^{-5} (5×), 8×10^{-6} (25×), and 2×10^{-6} (100×). In this calculation and subsequent use in the Monte Carlo simulations, the size distributions of the fabricated gold nanoshells were neglected and only the average size was considered. The optical properties of water were not considered in the final optical properties of the model because the experimental setup eliminates optical attenuation due to water. The nanoshell suspension was modeled as a semi-infinite homogenous (depth (d) = 1.0×10^8 cm) layer. As the nanoshell suspensions are diluted, the optical coefficients decrease proportionately as demonstrated by Eq. (2). The MCML method assumes that the angular scattering pattern of the turbid media follows the Henyey–Greenstein approximation (Henyey & Greenstein, 1941). It is also important that the angular scattering pattern of gold nanoshells can be approximated to the Henyey–Greenstein scattering pattern. Figure 4 shows the comparison between the actual angular scattering pattern and the scattering pattern approximated by Henyey–Greenstein. The graphs in Figure 4 show the scattering patterns of the R104/127 nanoshell at 630 nm (Figure 4(a)) and at 830 nm (Figure 4(b)). While there are small differences, gold nanoshell angular scattering is adequately estimated by the Henyey–Greenstein approximation.

Results

Figures 5 through 7 show the computational and experimental results of the R104/127, R71/84 and R154/178 nanoshells, respectively. To avoid confusion, features from the measured reflectance spectra related to photon scattering from large angles (~180°) will hereinafter be referred to as Large Angle Scattering (LAS). Graphs (a) and (b) in Figures 5–7 show the theoretical nanoshell

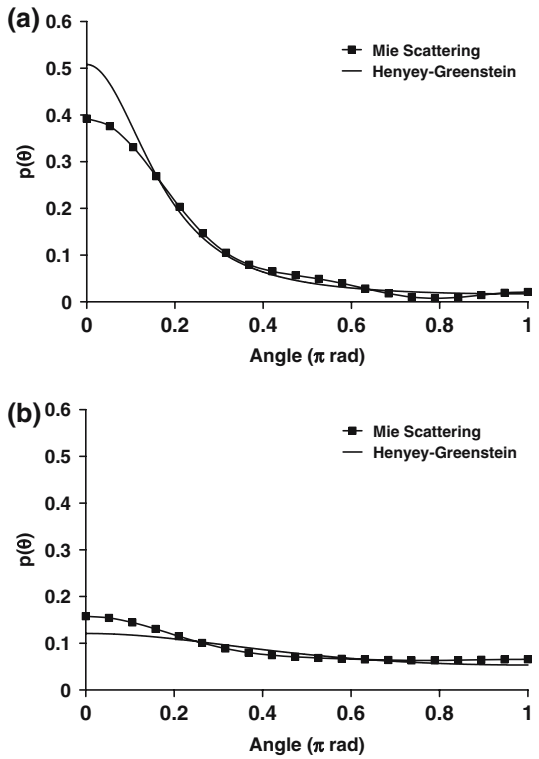

Figure 4. Graphs shows the angular scattering patterns of the R104/127 gold nanoshell at (a) 630 nm and (b) 830 nm. The graphs show that the theoretical Mie scattering patterns is adequately estimation by the Henyey–Greenstein phase scattering approximation, and thus appropriately modeled in Monte Carlo.

optical properties calculated from Mie theory. Figures 5(a), 6(a) and 7(a) show the scattering, absorption, extinction and 180-Scattering (van der Hulst, 1981 (efficiencies as a function of wavelength and Figures 5(b), 6(b) and 7(b) shows the anisotropy parameter (g value) as a function of wavelength. Spectroscopy measurements of gold nanoshell suspensions diluted from $1\times$ to $100\times$ are shown in Figures 5(c), 6(c) and 7(c). The Monte Carlo simulation results for each nanoshell are shown in Figures 5(d), 6(d) and 7(d). To further analyze the modeling results, Figure 8 shows the percent reflectance as a function of the collection radius at 700 nm over the first 500 μm radius of the R71/84 nanoshell suspension model. In the graph (Figure 8), 0 μm represents the point of photon packet introduction (POI), and the x-axis (radius) is the distance from POI at which the reflectance is recorded. It is important to note that the total reflectance remains the same for the different dilutions modeled (Figure 6(d)). Each data point in Figure 8 represents the modeled reflectance accumulated from each 50 μm interval and is represented at the midpoint. The insert in Figure 8, shows the accumulated modeled reflectance collected over the first 500 μm radius as a percentage of the modeled total diffuse reflectance that was collected regardless of radial distribution. Figure 9 shows the accumulated diffuse reflectance collected from a radius of > 500 μm, with respect to volume fraction of the R71/84 gold nanoshell.

Discussion

Diffuse reflectance spectroscopy

Scattering and absorption

From the results shown in Figures 5–7, a marked change in diffuse reflectance was observed, particularly for longer wavelengths in all the nanoshells used in our studies. From these results, nanoshells that exhibit high scattering, with low absorption and low anisotropy, generally exhibit substantial changes in measured diffuse reflectance. In general, then, we can say that higher scattering and lower absorption efficiencies will result in higher measured reflectance. However, it should be added that this generalization is complicated by the changing anisotropy factor across the spectral range, which is explained below.

Anisotropy parameter (g)

The anisotropy parameter, g, a dimensionless number, is a measure of the photon travel direction retained after a single scattering event and is the expectation value for average $\cos(\theta)$ shown in Figures 5(b), 6(b) and 7(b). The value of g ranges from -1 to 1, with a positive value indicating the preference for forward scattering and a negative value for backward scattering. A value of 0 indicates isotropic scattering and equal probability of scattering in all directions. The nanoshells used in our studies have anisotropy values that change with wavelength. This results in photons that are more backward scattering and, hence, the phenomenon contributes to the overall measured reflectance. As shown in Figures 5(c), 6(c) and 7(c), at $V_f = 0.0002$, the R71/84 nanoshell shows

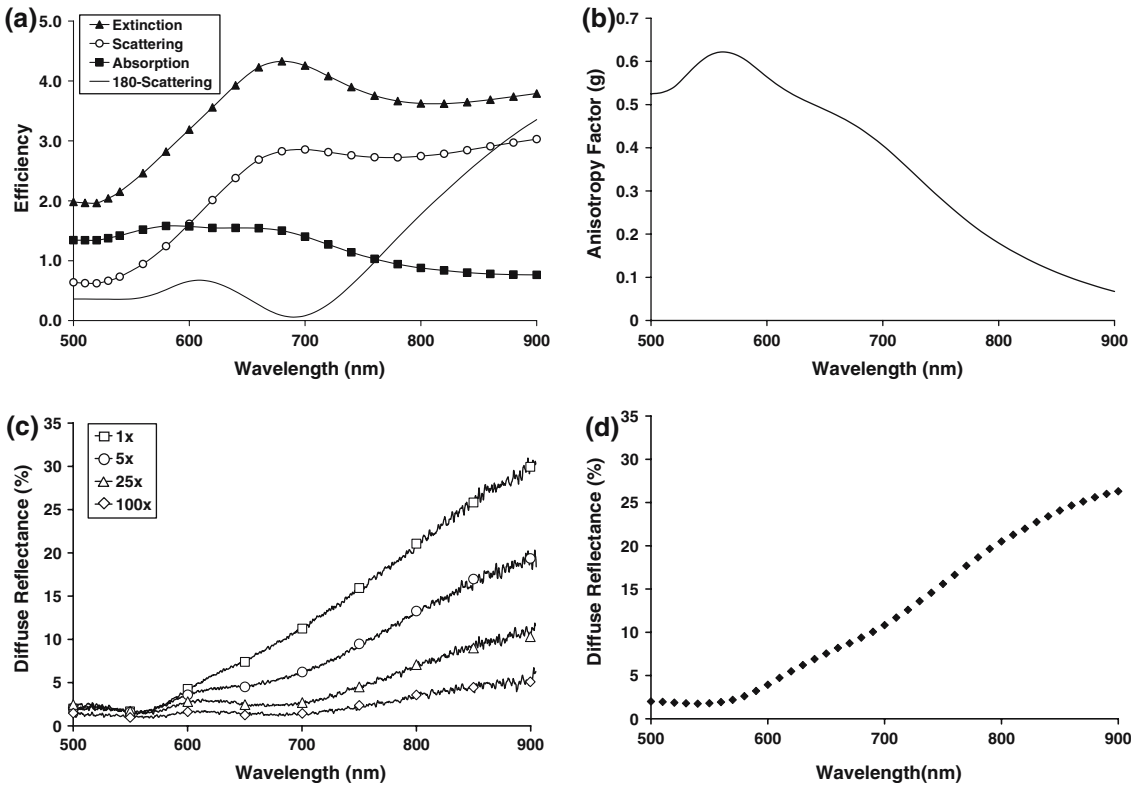

Figure 5. Graphs show computational and experimental results from the R104/127 nanoshell. Graph (a) shows the scattering, absorption, extinction, and 180-Scattering (Scattering from 180°) properties calculated from Mie Theory. From Mie calculations, we can also obtain the anisotropy parameter (g) shown in graph (b). Diffuse reflectance spectroscopy experiments of diluting gold nanoshell suspensions are shown in graph (c). Diluting the suspension by 5×, 25× and 100× shows decreasing detected reflectance. Using Monte Carlo computational methods, diffuse reflectance of the R104/127 nanoshell suspended in water is simulated. Results only show one representative line, while the total reflectance of diluting a suspension remains the same.

a diffuse reflectance of approximately 15% within the 800 nm to 900 nm wavelength region, while the R154/178 nanoshell also shows reflectance approximately 15% within the same wavelength region. This occurs despite that the R154/178 nanoshell shows higher scattering efficiencies and lower absorption efficiencies compared to the R71/84 nanoshell. This discrepancy is likely a result of the lower anisotropy values at 800 nm to 900 nm of the R71/84 nanoshell as compared to the R154/178 nanoshell.

Large angle scattering (LAS)

As nanoshell suspensions are diluted, the inter-particle distance between nanoshell particles increases causing the number of detectable LAS photons to increase. As the particles are farther apart, photons scattered from large angles (~180°) are more likely to travel directly to the collection fiber without interacting with any other particle. This gives rise to spectral features that are more obvious at lower nanoshell concentrations. These features observed at lower concentrations can be related to the Q_{180} scattering efficiencies (Mie scattering solution at 180°) of nanoshells shown in Figures 5(a), 6(a) and 7(a) and which can be representative of photons scattered at approximately 180°. The R104/127 nanoshell shows a small reflectance peak at approximately 610 nm that is more noticeable at dilutions greater than 25× (Figure 5(c)), and this peak is seen in the 180-Scattering efficiencies shown in Figure 5(a). Similarly, the R154/178 nanoshell shows two peaks, one at ~590 nm and another at ~730 nm,

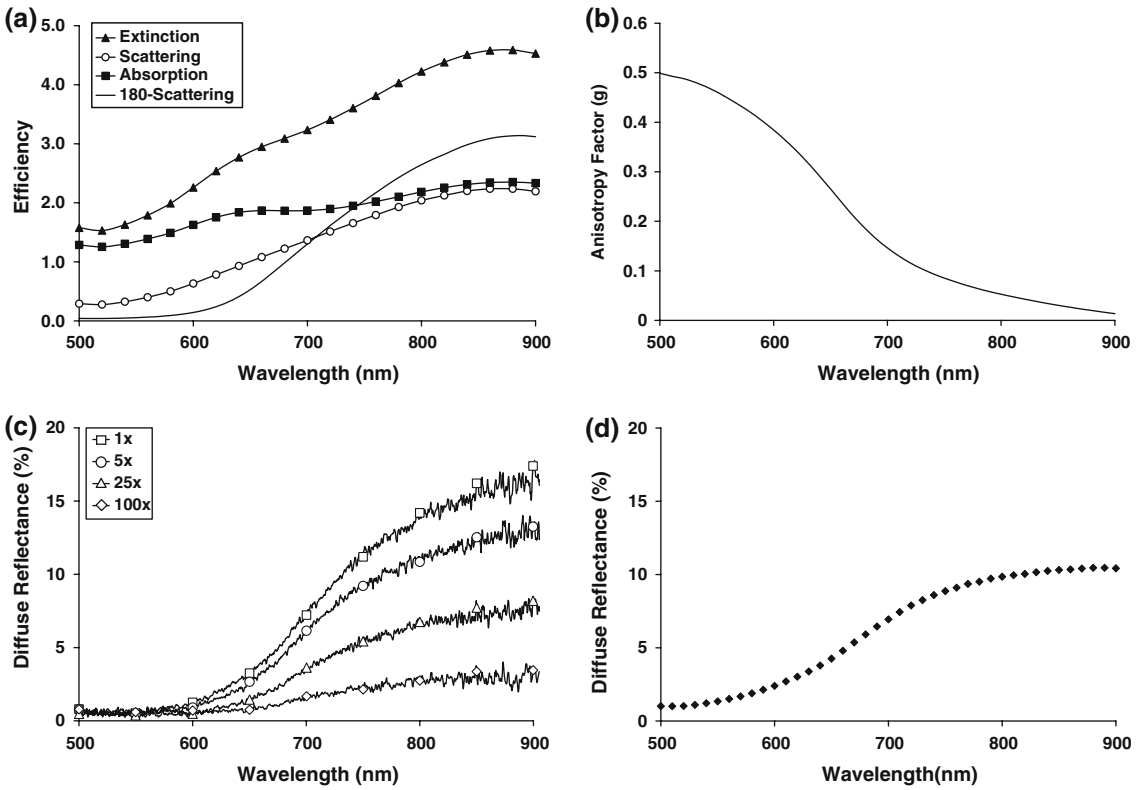

Figure 6. Graphs show computational and experimental results from the R71/84 nanoshell. See description for Figure 3.

where the peak at ~710 nm was only observed at dilutions greater than 5× (Figure 7(c)). The peak at ~710 nm corresponds to the peak seen in the 180-Scattering efficiency shown in Figure 7(a).

Monte Carlo modeling

In the graphs shown in Figures 5(d), 6(d) and 7(d), the modeling results are shown for each nanoshell. The graphs show the total diffusely reflected photons collected regardless of the radial distribution; and the diffuse reflectance from different concentrations of nanoshell suspensions remains the same, and only a single line is shown in the results. Diffuse reflectance of a model generally remains the same if the μ_s-to-μ_a ratio (with other parameters constant) remains the constant. However, the experimental results show that the detected diffuse reflectance decreases as the concentration of the nanoshell suspension is lowered. In general, the modeling results correspond to the measured spectra at high concentrations, with variations due to both the influence of LAS and the variation in nanoshell size distribution from the fabrication process. Then, as the suspension concentration is lowered, the detected reflectance signal appears to show an increase in photons that were scattered from large angles (~180°). To investigate how decreasing nanoshell concentration affects the reflectance signal collected, we first analyzed the radial distribution of the measured diffuse reflectance up to 500 μm from the POI (see Figures 3 and 8). From Figure 8, the 1× suspension shows the greatest change in reflectance over the first 200 μm radius, and at lower concentrations, while the reflectance remains low and more evenly distributed through 500 μm. To further analyze photon distribution, Figure 9 shows the accumulated diffuse reflectance of all reflected photons at any distance greater than 500 μm as a function of the volume fraction (R71/84). The most dilute nanoshell suspensions show the highest accumulated diffuse reflectance for distances >500 μm. With decreasing volume fraction, a

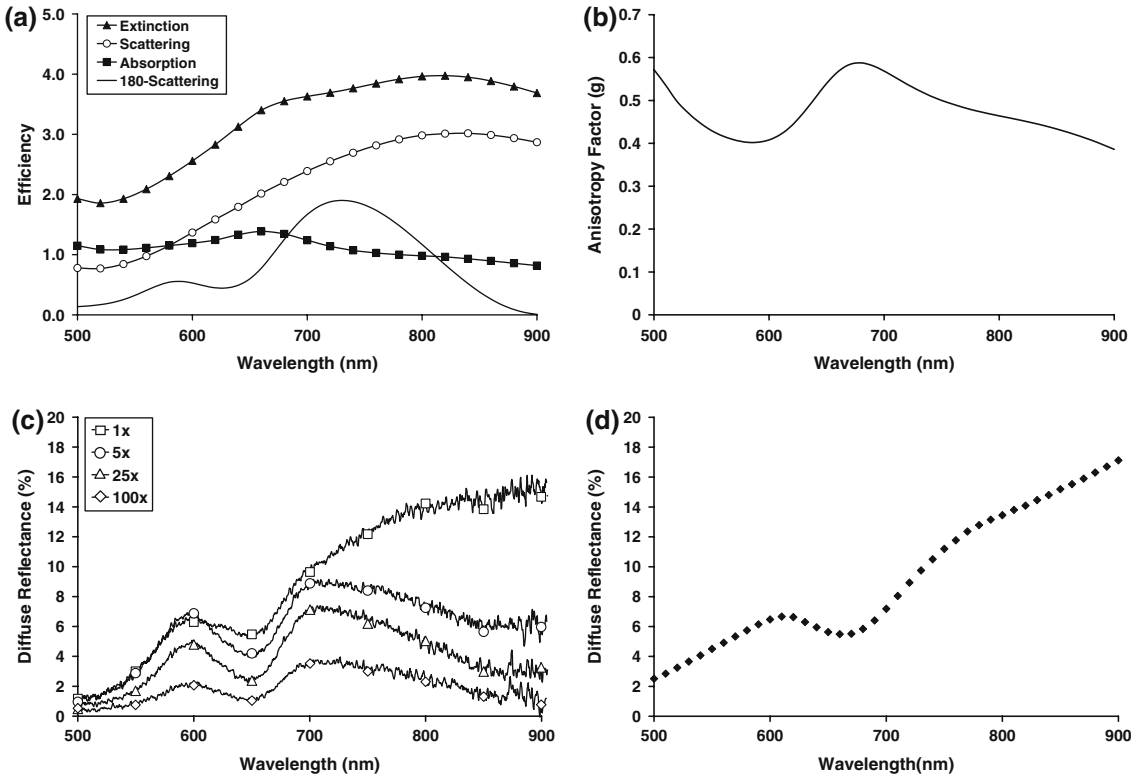

Figure 7. Graphs show computational and experimental results from the R154/178 nanoshell. See description for Figure 3.

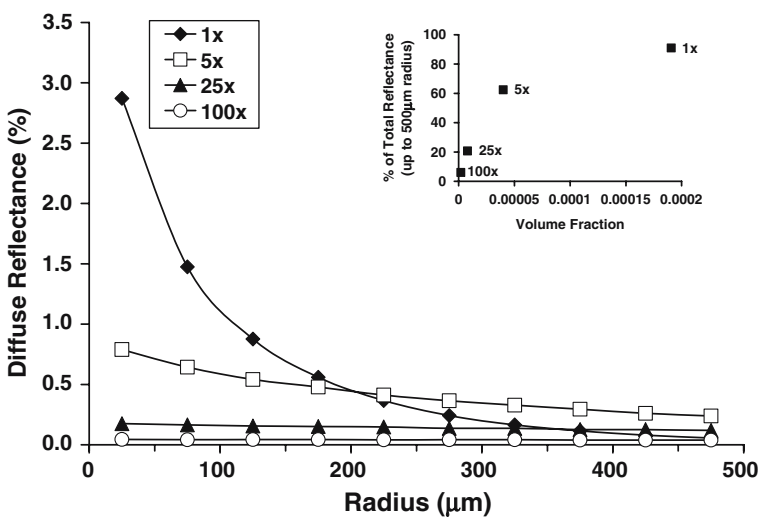

Figure 8. Using the results from the Monte Carlo computations, the distribution of photons across the collection radius is analyzed. The graph shows the accumulated reflectance, at 50 μm intervals up to 500 μm, of the R71/84 nanoshell dilutions at 700 nm excitation wavelength and where 0 μm represents the point where photon packets are introduced. It is important to remember that, regardless of distribution, the total reflectance remains the same for the dilutions of the same nanoshell suspension. The insert shows the accumulated reflectance of photons from radial distances less than 500 μm as a percentage of the total modeled reflectance. At 1× concentration, this is almost 100%, and therefore the modeled reflectance (Figures 5(d), 6(d) and 7(d) corresponds to experimental measurements of highly concentrated gold nanoshell suspensions.

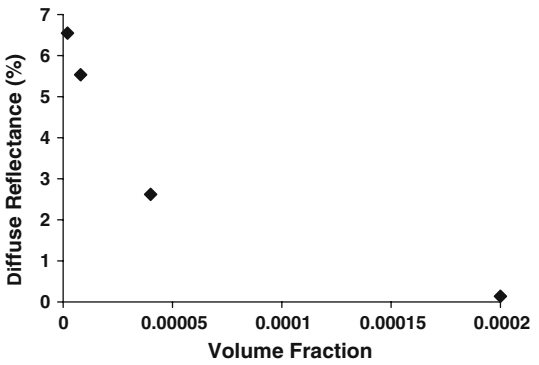

Figure 9. Graph shows that a greater proportion of photons is reflected farther away from the source when all the photons remitted at > 500 μm for the R71/84 nanoshell are accumulated. As the volume fraction of nanoshells decreases, a greater number of photons are remitted > 500 μm.

greater proportion of photons are remitted further away from the POI (> 500 μm); at the same time, as the extinction coefficient decreases, an increasing effective photon pathlength results. In order to understand why the experimental results correspond more closely to the modeled total reflectance at higher nanoshell concentrations, we analyzed the distribution of the photon reflectance. From the insert shown in Figure 8, the modeled diffuse reflectance collected from a radial distance less than 500 μm from the POI of the 1× nanoshell suspension is almost 100% of the total reflectance, whereas, the 100× suspension shows only about 6% of the total modeled reflectance. From the modeling results, we can infer that, in the experimental measurements, the fiber optic probe (diameter of collection fiber = 400 μm) detect most of the diffusely reflected photons from a highly concentrated suspension of gold nanoshells.

In summary, when the results from the modeling and spectroscopy studies are compared, the experimental observation demonstrates that decreasing nanoshell concentrations appear to decrease the measured diffuse reflectance. Analysis of the photon distribution of the Monte Carlo models suggests that the experimental observations of decreasing diffuse reflectance are due, in fact, to the fixed fiber-probe geometry. In the spectroscopy measurements, the source-detector separation distance (distance between the source fiber and the collection fiber) of the probe is constant and can only collect photons up to a fixed distance. When the nanoshell volume fraction is lowered, the fiber-probe detects decreasing diffuse reflectance, where a greater proportion of reflected photons is not detected at all by the probe.

Conclusions

The unique, tunable and strong optical responses of gold nanoshells, particularly in the NIR, are most desirable for biophotonics applications. Gold nanoshell optical properties have already been widely reported and are typically shown in transmission. In this paper, we show both experimental and modeling analysis of gold nanoshell reflectance. As gold nanoshell reflectance has not yet been investigated, it is important to understand how tissue reflectance will be altered when used in conjunction with scattering-based spectroscopic methods for the detection of cancers targeted by gold nanoshells. From our studies, we show that gold nanoshells with high scattering efficiencies and low anisotropy parameter values (g) of nanoshells are ideal for producing a significant increase in diffuse reflectance. The high scattering efficiencies at 180 degrees (Q_{180}) were observed to significantly alter scattering signatures, especially at lower concentrations. This important property has already been shown to improve contrast for scattering-based imaging with OCT (Barton et al., 2004; Agrawal et al., 2006). From the Monte Carlo studies, gold nanoshell reflectance can be accurately modeled as a homogenous medium and may be useful for modeling reflectance of tissue with embedded gold nanoshells. In this paper, we have also shown that gold nanoshells are an excellent candidate as an optical contrast agent for altering scattering signatures for scattering-based diagnostic modalities. Furthermore, the modeling method can be used to obtain optimized nanoshells best suited for scattering-based optical technologies.

Acknowledgements

We would like to acknowledge the following funding agencies for their generous support: National Science Foundation (BES 022–1544 and

EEC-0118007); DOD CDRMP DAMD17-03-1-0384; the Welch Foundation, and the Beckman Foundation.

References

Agrawal A., S. Huang, A. Lin, M.-H. Lee, J. Barton, R. Drezek & T. Pfefer, 2006. J. Biomed. Opt. (in press).

Akerman M.E., W.C.W. Chan, P. Laakkonen, S.N. Bhatia & E. Ruoslahti, 2002. Nanocrystal targeting *in vivo*. PNAS 99, 12617–12621.

Barton J.K., N.J. Halas, J.L. West & R.A. Drezek, 2004. Nanoshells as an optical coherence tomography contrast agent. Proc. SPIE Int. Soc. Opt. Eng. 5316, 99–106.

Brigger I., C. Dubernet & P. Couvreur, 2002. Nanoparticles in cancer therapy and diagnosis. Adv. Drug Delivery Rev. 54, 631–651.

Bohren C.F. & D.R. Huffman, 1983. Absorption and Scattering of Light by Small Particles. New York: John Wiley and Sons.

Chang E., J.S. Miller, J. Sun, W.W. Yu, V.L. Colvin, R. Drezek & J.L. West, 2005. Protease-Activated quantum dot probes. Biochem. Biophys. Res. Commun. 334, 1317–1321.

Chen J., F. Saeki, B.J. Wiley, H. Cang, M.J. Cobb, Z.-Y. Li, L. Au, H. Zhang, M.B. Kimmey, X. Li & Y. Xia, 2005. Bioconjugated gold nanocages and evaluation of their potential for optical imaging and thermal therapeutic applications. Nano. Lett. 5, 473–477.

Drezek R., T. Collier, C. MacAulay, M. Follen & R. Richards-Kortum, 2003. Light scattering from cervical cells throughout neoplastic progression: influence of nuclear size, DNA content, and chromatin texture. J. Biomed. Opt. 8, 7–16.

Duff D.G., A. Baker & P.P. Edwards, 1993. A new hydrosol of gold clusters. 1. Formation and particle size variation. Langmuir 9, 2301–2309.

Faulk W.T. & G. Taylor, 1971. An immunocolloid method for the electron microscope. Immunochemistry 8(11), 1081–1083.

Henyey L. & J. Greenstein, 1941. Diffuse radiation in the galaxy. Astrophys. J. 93, 70–83.

Kreibig U. & M Vollmer, 1995. Optical Properties of Metal Clusters. Berlin: Springer-Verlag.

Levy L., Y. Sahoo, K.-S. Kim, E.J. Bergey & P.N. Prasad, 2002. Nanochemistry: Synthesis and characterization of multifunctional nanoclinics for biological applications. Chem. Mater. 14, 3715–3721.

Licha K., 2002. Contrast Agents for Optical Imaging. Topics Curr. Chem. 222, 1–29.

Lin A.W.H, N.A. Lewinski, J.L. West, N.J. Halas & R.A. Drezek, 2005. Optically tunable nanoparticle contrast agents for early cancer detection: A model-based analysis of gold nanoshells. J. Biomed. Opt. 10, 064035.

Loo C., L. Hirsch, M. Lee, E. Chang, J. West, N. Halas & R. Drezek, 2004. Gold nanoshell bioconjugates for molecular imaging in living cells. Opt. Lett. 30(9), 1012–1014.

Loo C., A. Lin, L. Hirsch, M. Lee, J. Barton, N. Halas, J. West & R. Drezek, 2004. Nanoshell-enabled photonics-based imaging and therapy of cancer. Technol. Cancer Res. Treat. 3(1), 33–40.

Loo C., A. Lowery, N. Halas, J. West & R. Drezek, 2005. Immunotargeted nanoshells for integrated cancer imaging and therapy. Nano. Lett. 5(4), 709–711.

Matheny E.S., N.M. Hanna, W.G. Jung, Z. Chen, P. Wilder-Simth, R. Mina-Araghi & M. Brenner, 2004. Optical coherence tomography of malignancy in hamster cheek pouches. J. Biomed. Opt. 9(5), 978–981.

Michalet X., F.F. Pinaud, L.A. Bentolila, J.M. Tsay, S. Doose, J.J. Li, G. Sundaresan, A.M. Wu, S.S. Gambhir & S. Weiss, 2005. Quantum dots for live cells, in vivo imaging, and diagnostics. Science 307(5709), 538–549.

Oldenburg S.J., R.D. Averitt, S.L. Westcott & N.J. Halas, 1998. Nanoengineering of optical resonance. Chem. Phys. Lett. 288, 243–247.

Oldenburg S.J., J.B. Jackson, S.L. Westcott & N.J. Halas, 1999. Infrared extinction properties of gold nanoshells. Appl. Phys. Lett. 75(19), 2897–2899.

Sokolov K., M. Follen, J. Aaron, I. Pavlova, A. Malpica, R. Lotan & R. Richards-Kortum, 2003. Real-time vital optical imaging of precancer using anti-epidermal growth factor receptor antibodies conjugated to gold nanoparticles. Cancer Res. 63, 1999–2004.

Sokolov K., L.T. Nieman, A. Myakov & A. Gillenwater, 2004. Polarized reflectance spectroscopy for pre-cancer detection. Technol. Cancer Res. Treat. 3(1), 1–14.

Stober W., A. Fink & E. Bohn, 1968. Controlled growth of monodisperse silica spheres in the micron size range. J. Colliod Interface Sci. 26, 62–69.

Wang D., J. He, N. Rosenzweig & Z. Rosenzweig, 2004. Superparamagnetic Fe_2O_3 beads-CdSe/ZnS quantum dots core-shell nanocomposite particles for cell separation. Nano. Lett. 4(3), 409–413.

Wang L.H., S.L. Jacques & L.Q. Zheng, 1995. MCML- Monte Carlo modeling of photon transport in multi-layered tissues. Comput. Meth. Programs Biomed. 47, 131–146.

West J.L. & N.J. Halas, 2003. Engineered Nanomaterials for Biophotonics Applications: Improving sensing, imaging, and therapeutics. Annu. Rev. Biomed. Eng. 5, 285–292.

van der Hulst H.C., 1981 Light Scattering by Small Particles. New York: Dover Press.